This is a repository copy of *A chemical reaction driven untethered volume changing robotic capsule for tissue dilation*.

eprints@whiterose.ac.uk
https://eprints.whiterose.ac.uk/

A Chemical Reaction Driven Untethered Volume Changing Robotic Capsule for Tissue Dilation

Kaan Esendag[1], Mark E. McAlindon[2], Daniela Rus[3], Shuhei Miyashita[1,4,5], and Dana D. Damian[1,4,5]

Abstract—Robotic capsules provide an alternative route of entry to the gastrointestinal tract with minimal discomfort to patients. As capabilities of milli to micro robots progress, the potential of using robotic capsules not just for inspection, but for surgical procedures increase. To aid operations in the intestine, the capsule could be used to expand the site of surgery and anchoring to the intestinal walls to keep itself in place. This paper presents an untethered robotic capsule that can provide volumetric expansion using a chemical reaction without on-board electronic components. The expansion is based on the reaction between chemicals that are safe for ingestion, operated with magnetic fields and temperatures that are within safe limits. The capsule was able to expand greater than the diameter of the small intestine for 44 minutes and provided 0.27 N of anchoring force. A theoretical model of the reaction process was built and simulated to predict the behavior of the capsule expansion and validated through the experiments. The design and the simulation presented in this paper can be used for fabricating capsules to specific clinical needs. The work also opens up the possibility of untethered technologies that are remotely and chemically programmed for in-vivo surgical applications.

Index Terms—Robotic Capsule Devices, Inflatable Actuator, Untethered, Magnetic Induction, Chemical Reaction, Dissolution, Chemical programming.

I. INTRODUCTION

ROBOTIC capsules provide alternative methods to minimally invasive procedures in the gastrointestinal tract such as endoscopy, colonoscopy and laparoscopy, which can further reduce the invasiveness. While the current state-of-the-art for robotic capsules fulfills the need for inspection [1], sample collection [2], [3] and targeted local drug administration [4]–[8], a gap still exists between the capabilities of robotic capsules and tethered surgical solutions [9]–[11]. Inclusion of small scale tools such as cutters [12], forceps [13], manipulators [14] and biopsy needles [2] in robotic capsules could enable untethered surgical procedures to be performed in the gastrointestinal tract. In order to use these tools in the small intestine, a capsule needs to dilate the site of surgery greater than the diameter of the small intestine (25-30 mm [4]), and anchor to the tissue for long periods of time as inspection

[1] Automatic Control and Systems Engineering Department, University of Sheffield, Sheffield S1 3JD, UK (e-mail: kesendag1@sheffield.ac.uk; d.damian@sheffield.ac.uk).
[2] Royal Hallamshire Hospital, Sheffield Teaching Hospitals NHS Foundation Trust, UK
[3] MIT Computer Science and Artificial Intelligence Laboratory (CSAIL), Massachusetts Institute of Technology, Cambridge, MA 02139 USA.
[4] Insigneo Institute for in silico Medicine, University of Sheffield, UK.
[5] Sheffield Robotics, University of Sheffield, UK.

can take around 20 minutes [15] and surgical procedures can take around 50 minutes [16].

As a method of dilation, robotic capsules featuring mechanical legs have been developed [4], [17]. The small contact surface area provided by the legs greatly increases the local pressure applied on the anchored tissue with the risk of tissue puncture. Capsules which dilate and maintain a compliant interface are safer in this regard. An example of an untethered inflatable ballooning mechanism is presented in [18], which uses a chemical reaction as its source of pressure, however little consideration is given to the controllability of the changing capsule volume. Moreover, inclusion of electronic components, motors or batteries generally results in large and overweight capsules. A completely electronics-free volume changing soft actuator was developed using the phase transition of low-boiling point liquids [19], [20], but the operation temperature goes beyond the limits of cell necrosis which is around 45 °C [21], [22] and the actuator can only be inflated for brief periods of time.

As contributions, this paper presents:

1) Concept of a novel electronics-free volume-changing capsule device using a mechanism of wirelessly regulating a chemical reaction to control the volume of produced gas.
2) Modeling of the chemical reaction process which causes the inflation and deflation of the capsule.
3) Validation of the performance in experiments and comparison with simulation results.

II. METHODS

A. Design Concept and Specification

The overview of the capsule operation is shown in Fig. 1. In stage 1, the capsule is navigated to the surgical site, using a magnet attached inside it. The capsule remote navigation was demonstrated by our group in [23], and more widely in [24]. The capsule holds reactants for the gas-generating chemical reaction in gelatin rings, isolated from each other. The capsule also has a copper sheet wrapped around the gelatin rings and contains water which acts as a solvent. In stage 2, the capsule's inflation is wirelessly controlled through magnetic induction which generates thermal energy in the copper sheet and dissolves the gelatin. The release of reactants lead to the chemical reaction which produces carbon dioxide (CO_2) gas for capsule inflation. The reactants chosen for the chemical reaction are citric acid ($C_6H_8O_7$) and sodium bicarbonate ($NaHCO_3$), which are safe for consumption [25], [26]. The alternating magnetic field used in induction heating
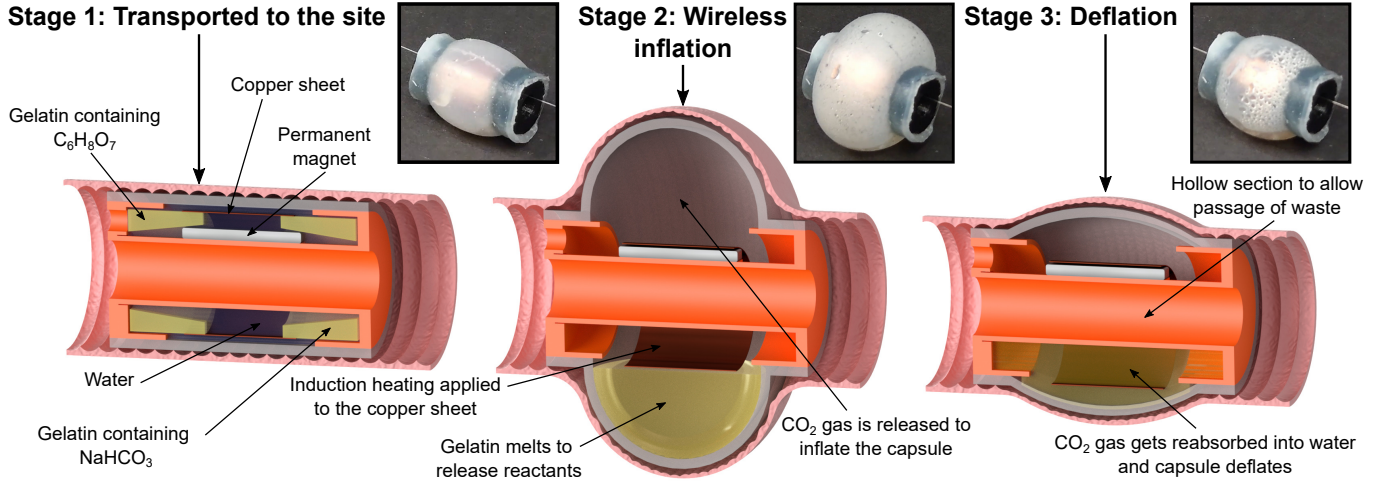
Fig. 1. CAD renders showing a cross-section view of the robotic capsule in a section of intestine, along with real images of the capsule. The concept diagram is broken down into three stages along a timeline. First the robotic capsule reaches the site of surgery, then induction heating is applied to control the actuation, the chemical reaction takes place to inflate the capsule, followed by the reabsorption of CO_2, deflating the capsule to leave the site of surgery.

has a peak amplitude of $5\,mT$ oscillating at $27\,kHz$ which is considered to be low frequency and amplitude when compared with similar methods [19], [20], [27], [28]. The induction coil is located $4\,cm$ below the capsule which is a similar distance compared to literature given that the peritoneal cavity from the neutral position is $30.9\,mm$ [29]. In stage 3, the capsule undergoes deflation. As the capsule cools down, the produced gas is absorbed into the water and the capsule deflates to its original volume. The inflation is controlled by a magnetic field below the Brezovich limit [22]. The proposed method hence provides a safer, novel and promising alternative for surgical in-vivo operations, especially those that require prolonged usage.

B. The Volume Changing Mechanism

This section investigates the magnetic induction driven chemical reaction used to actuate the capsule and identify the underlying control variables. To control the rate and timing of the chemical reaction, each of the reactants is stored separately in solid rings of gelatin to prevent their mixing. When thermal energy is generated in the copper sheet, the gelatin rings slowly dissolve in water inside the capsule, gradually releasing reactants into the aqueous solution. The deflation of the capsule is due to the CO_2 gas being slowly reabsorbed into the water and broken down into carbonic acid (H_2CO_3). The interactions between these variables, separated into three aspects: temperature, chemical reaction and gas production, are explained in Fig. 2. In the following model, we determined some parameters, as specified below, from empirical measurements (see Fig. 6, Experiment A). The resulting model was then used to validate experimental results of Experiment B in Fig. 6.

1) Temperature: When alternating magnetic fields are applied to the capsule, eddy currents are produced in the copper sheet inside the capsule, which generate thermal energy by

Joule heating. The energy generated by the eddy currents per unit mass of conductor, Q_e (J kg^{-1}), is [30]:

$$Q_e = \frac{\pi^2 \sigma B_p^2 h^2 f}{6\rho_c} \quad , \quad (1)$$

where σ is the conductivity of the copper sheet ($5.95 \times 10^7\,\Omega^{-1}\,m^{-1}$), B_p is the peak magnetic flux density applied (T), h is the thickness of the copper sheet (m), f is the frequency of the magnetic waves (Hz) and ρ_c is the density of the copper sheet ($8960\,kg\,m^{-3}$).

This energy can be multiplied by the frequency and the mass of the copper sheet to get the power input to the system, P_{in} (W), at any given time is:

$$P_{in} = \frac{\pi^2 \sigma B_p^2 h^2 f^2 m_c}{6\rho_c} \quad , \quad (2)$$

where m_c is the mass of the copper sheet (kg).

The power input to the system is multiplied by the duration the magnetic field is applied for. When the temperature of the capsule is T (°C), the temperature increase caused by eddy currents when there is no heat dissipation, ΔT (°C), can be described as:

$$\Delta T = \frac{P_{in}\Delta t}{m_c c_{p(c)}} = \frac{\pi^2 \sigma B_p^2 h^2 f^2 \Delta t}{6\rho_c c_{p(c)}} \quad , \quad (3)$$

where Δt is time (s) and $c_{p(c)}$ is the specific heat capacity of the conductor ($389\,J\,kg^{-1}\,°C^{-1}$).

The system dissipates a portion of excess heat to the environment. While there exists many factors that affect the rate of heat loss, the rate was taken as a constant with reference to our experiments. The change of temperature due to heat dissipation to the environment over Δt is:

$$\Delta T = T - T_{env} - (T - T_{env})e^{-2.80\times 10^{-4}\Delta t} \quad , \quad (4)$$

where T_{env} is the environmental temperature (°C). The decay value was determined by applying induction heating to the capsule, recording the thermal loss, then curve fitting to the measured results (see Fig. 6, Experiment A conditions).
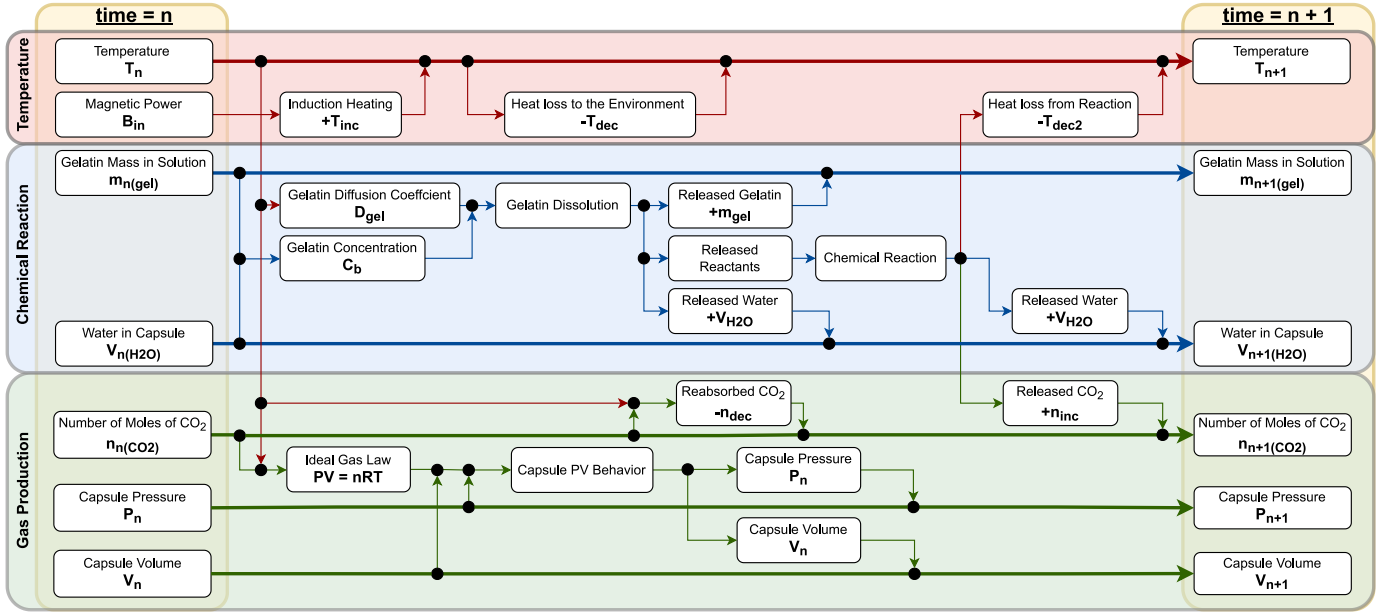
Fig. 2. Flow diagram of the simulation of inflation mechanism, showing the interaction between different variables of the theoretical model. The interaction is broken down into three aspects: temperature, chemical reaction and produced CO_2 modeled as an ideal gas inside the capsule. The inputs at time n are used to predict the outputs at time $n + 1$.

2) Chemical Reaction: Thermal energy input is needed to dissolve gelatin and the reactants it contains from a solid into a liquid. The dissolution rate of gelatin relies on the diffusion coefficient which is a function of its temperature, viscosity of solvent and hydrodynamic radius of the solute, where the latter two variables also depend on temperature. The Stokes-Einstein equation was used with the hydrodynamic radius of gelatin [31] and viscosity of water [32] at different temperatures, to calculate the diffusion coefficient of gelatin for a range of $35 \leqslant T_n < 60\,°C$. The results were curve-fitted to get the diffusion coefficient of gelatin, D_{gel} ($m^2\,s^{-1}$), which is defined by:

$$D_{gel} = 3.07 \times 10^{-12} e^{0.0369T} . \qquad (5)$$

Applying the Noyes-Whitney equation of dissolution, we obtained the dissolution rate of gelatin in water [33]. The mass of gelatin that will dissolve in water, m_{gel} (g), can be described as:

$$\Delta m_{gel} = \frac{A_{gel} D_{gel}}{d_{gel}} \left(C_s - \frac{m_{gel}}{V_{H_2O}} \right) \Delta t, \qquad (6)$$

where A_{gel} is the surface area of the dissolving gelatin in contact with water (cm^2), D_{gel} is in $cm^2\,s^{-1}$, d_{gel} is the diffusion distance between gelatin and water (cm), C_s is the saturation concentration of gelatin ($g\,ml^{-1}$) and V_{H_2O} is the volume of water inside the capsule (ml). d_{gel} and C_s were computationally determined to be 1.5×10^{-4} cm and $0.067\,g\,ml^{-1}$ respectively, by incrementally changing d_{gel} and C_s, and comparing theoretical results with measured values from Fig. 6, Experiment A conditions, until the curves match.

When the gelatin dissolves, the reactants are released into the solvent, the amount of which can be determined using the ratio of ingredients that was used to make the gelatin rings. The gas-producing reaction between $NaHCO_3$ and $C_6H_8O_7$

increases the volume of the capsule and the pressure inside it. Using the amount of $NaHCO_3$ that would be released through the gelatin ring dissolution, the number of moles of CO_2 gas inside the capsule, n_{CO_2} (mol), that will be produced as a product of the chemical reaction is derived as:

$$\Delta n_{CO_2} = \frac{m_{NaHCO_3}}{3\,M_{NaHCO_3}} \quad , \qquad (7)$$

where m_{NaHCO_3} is the mass of $NaHCO_3$ released from the gelatin ring dissolution (g), M_{NaHCO_3} is the molar mass of $NaHCO_3$ ($389\,g\,mol^{-1}$).

The chemical reaction also releases water, so the released water can be added back to the water already in the capsule:

$$\Delta V_{H_2O} = \frac{m_{NaHCO_3} 3\,M_{H_2O}}{3\,M_{NaHCO_3}} \quad , \qquad (8)$$

where M_{H_2O} is the molar mass of H_2O ($18\,g\,mol^{-1}$).

Even though the formation of CO_2, H_2O and trisodium citrate ($Na_3C_6H_5O_7$) is exothermic, the dissociation of $Na_3C_6H_5O_7$ into sodium and citrate ions as well as gas evolution from the formation of CO_2 are endothermic, which results in the overall chemical reaction to be endothermic.

The decrease in temperature due to the energy absorbed per mole of reaction can be given by:

$$\Delta T = Q_r \frac{m_{NaHCO_3}}{M_{NaHCO_3}\,c_{p(H_2O)}\,\rho_{H_2O}\,V_{H_2O}} \quad , \qquad (9)$$

where Q_r is the resulting energy loss per mole of reaction (J), $c_{p(H_2O)}$ is the specific heat capacity of water ($4182\,J\,kg^{-1}\,°C^{-1}$) and ρ_{H_2O} is the density of water ($1\,g\,ml^{-1}$). Q_r was experimentally measured to be approximately $40\,kJ$ by mixing the reactants and measuring the temperature drop.

3) Gas Production: As the n_{CO_2} increases, the pressure and volume increases. The change in product of absolute pressure and volume inside the capsule chamber, PV ($Pa\,m^3$), can be calculated using the ideal gas law:

$$\Delta PV = \Delta n_{CO_2} R \Delta T \quad , \qquad (10)$$

where R is the ideal gas constant ($8.31\,J\,K^{-1}\,mol^{-1}$).

The following formula describes the relationship between absolute pressure, P (Pa) and volume, V (m^3), that is valid for the current capsule design:

$$P = 102.3\,e^{7.71\times10^{-7}V} - 1.12\,e^{-0.548V} \quad . \qquad (11)$$

The values were obtained by curve fitting to the data collected by applying a known volume of gas into the capsule for a range of $0 \leqslant V < 30\,ml$ and measuring the pressure.

In the capsule deflation stage, the rate of CO_2 reabsorption is described as:

$$\Delta n_{CO_2} = n_{CO_2} - n_{CO_2}e^{n_{decay}\Delta t} \quad , \qquad (12)$$

where n_{decay} is a variable that determines the reabsorption rate of CO_2. The reabsorption rate is dependent on the temperature. The formula for n_{decay} was estimated to be:

$$n_{decay} = -739\,e^{-0.630T} - 8.63 \times 10^{-4}e^{-2.54\times10^{-2}T} \quad . \qquad (13)$$

This relation was drawn experimentally by monitoring volume, temperature and pressure of the capsule during deflation which were used to estimate the number of molecules of CO_2 for a range of $25 \leqslant T_n < 40\,°C$ (data is presented in Experiment A in Section 3).

4) Time: In Fig. 2, the sequence of interactions in the simulation are represented between time T_n $\{n \in 1, 2, ...\}$ and T_{n+1}, where the Δt is $T_{n+1} - T_n$. The Δt used was 60 seconds. The output temperature at time $n + 1$ can be defined by:

$$T_{n+1} = T_n + T_{inc} - T_{dec} - T_{dec_2} \quad , \qquad (14)$$

where T_{inc} is the temperature increase due to eddy currents, T_{dec} is the heat loss to the environment and T_{dec_2} is the heat loss due to the chemical reaction.

The number of moles of CO_2 inside the capsule at time $n + 1$ can be defined by:

$$n_{n+1(CO_2)} = n_{n(CO_2)} + n_{inc} - n_{dec} \quad , \qquad (15)$$

where n_{inc} is the increase of CO_2 due to reaction, and n_{dec} is the CO_2 decrease due to reabsorption.

The theoretical model can be used to simulate the volume output of the capsule actuation to optimize the design parameters. For example, with increasing temperature, the rate of CO_2 production increases whereas the rate of CO_2 reabsorption decreases. Fig. 3 shows how the capsule actuation changes with applied magnetic flux density for a range of 0 to 10 mT which highlights how one variable can change the output considerably. For example, the melting point of gelatin is lower than the body temperature, which results in the capsule still reaching a peak of 6 ml of volume increase without any external heat input, but it reaches this volume

in 1 hour. Comparing this result with 10 mT input, the peak volume increases to 14 ml and happens at around 17 minutes, but the time spent at this peak is also reduced as well. Given that thermal input is an external, post-fabrication variable into the system, a single capsule design can be used for a range of clinical needs.
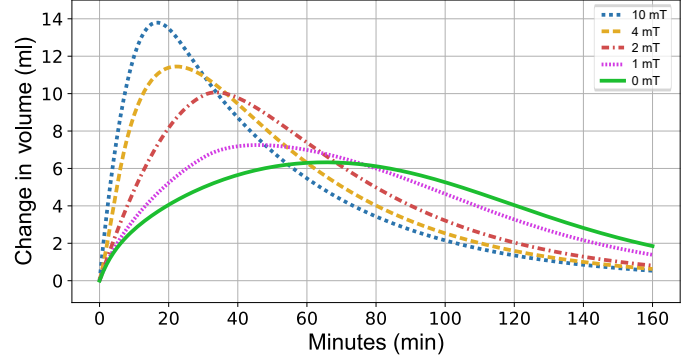

Fig. 3. Simulation results of the volume changing capsule reacting to a range of applied magnetic flux densities for 30 minutes of induction heating.

C. Capsule Design

The solid components of the capsule and the assembly order is shown in Fig. 4. The inner component of the capsule is the rigid body, which limits the capsule to only expand radially. The hollow section in the center allows passage of food or surgical tools through. A neodymium magnet of $12.7 \times 3.2 \times 1.5\,mm$ length, width and height respectively, is glued offset towards one side of the capsule on the rigid body for navigation.
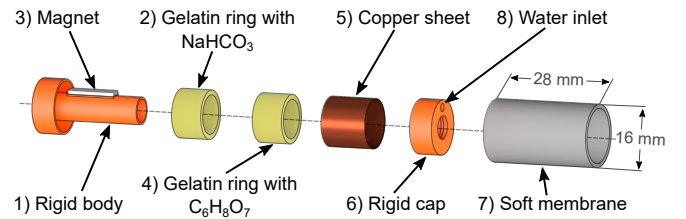

Fig. 4. Exploded view of the capsule showing the order of assembly.

For the fabrication of both the gelatin rings, two mixtures of gelatin and water were prepared according to the gelatin ring ratios described in Table I. The ratios were determined through systematic experimentation to yield a correct consistency that retains the reactants. The mixtures are heated in an oven at $60\,°C$ until they are fully melted. Then the reactants are added to their respective mixtures and poured into ring-shaped molds separately. After refrigerating for about 10 minutes, the gelatin rings are inserted around the rigid body. A 0.1 mm thick copper sheet is wrapped around the rings. Then the rigid cap is glued on the other end of the rigid body with cyanoacrylate. Both the rigid body and rigid cap are made of PLA using FDM printing.

The soft membrane that forms the ballooning body outside the capsule is made out of 1 mm thick Ecoflex 00-30 (Smooth
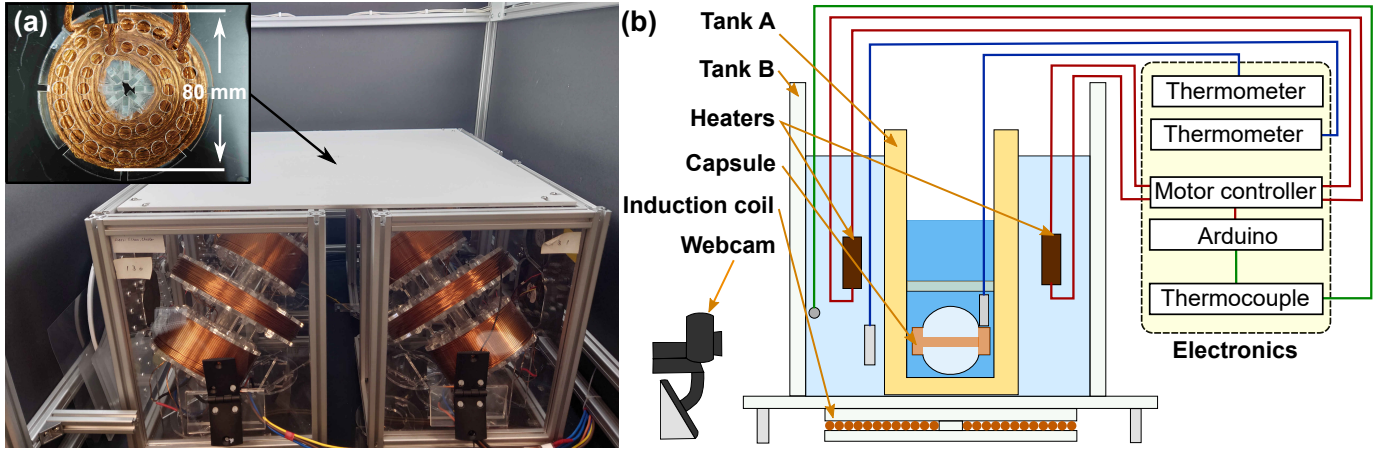
Fig. 5. (a) The induction coil (top left) and the navigation coils. The black arrow points at the location under which the induction coil is located. (b) The experimental setup used in the trials, with a block diagram for the electronics (The experimental setup can also be seen in the supplementary video).

On Inc.). It is wrapped around the rest of the capsule and a knot is tied around the circular edges. A thin layer of cyanoacrylate is applied between the soft membrane and the rigid body while the knot prevents the membrane from slipping. The same process is repeated for the other end. Ecoflex 00-30 is a biocompatible silicon [34]–[36] that is chemically inert with weak acids like citric acid and carbonic acid. For the final step, the capsule is filled with 2 ml of water through the inlet in the rigid cap, then sealed off. The capsule is kept frozen to avoid the gelatin from spoiling and can be defrosted before deployment. The capsule has a diameter of 16 mm, a length of 28 mm, and a weight of 6.65 g.

TABLE I
GELATIN RING PROPORTIONS BY MASS

Gelatin ring with reactant	Gelatin	Water	Reactant
$C_6H_8O_7$ (mg)	170	384	128
$NaHCO_3$ Mass (mg)	102	460	153

III. EXPERIMENTAL SETUP

An experimental setup that can provide an alternating magnetic field for at least 30 minutes was needed to test the actuation of the capsule. To provide alternating magnetic fields, we built a custom transmission coil for induction heating using braided litz wire, along with a Zero Voltage Switch (ZVS) circuit to supply alternating current. The specifications of the electronics design is shown in Table II.

Instead of using a solenoid coil design where the capsule needs to be through the solenoid for high power transfer efficiency, we chose a flat coil design shown in Fig. 5 (a) where all coil turns are on the same level, so the magnetic fields can be concentrated on a smaller area. This means that the capsule could be localized [37] and the induction coil could be placed at the closest position to the capsule in a more targeted manner to reduce the risk of non-specific tissue heating. The area of the coil covered by the nth number of turn, A_n (m^2) is:

$$A_n = \pi(r_c + Nd_w)^2 \quad , \tag{16}$$

TABLE II
INDUCTION COIL SPECIFICATIONS

Description	Value
MOSFETs used for ZVS circuit	STP60NF06
Total capacitance of ZVS resonant tank	2.2 μH
Induction coil inductance	15.4 μH
Resonant frequency	27 kHz
Target's vertical distance from center of coil	4 cm
Current buildup in the resonant tank	20 A
Peak Magnetic Flux density measured at center	5.5 mT
Induction coil inner diameter	27 mm
Induction coil outer diameter	80 mm
Litz wire individual strand diameter	0.2 mm
Number of strands in litz wire	100
Litz wire diameter total	3 mm
Number of turns in a single layer	12

where r_c is the inner radius of the coil (m), N is the number of turns equal to the n of A_n and d_w is the diameter of the litz wire (m). The inductance of a single layer coil, L (H), can be given by:

$$L = \frac{\mu_0(A_0 + A_1 + ... + A_n)}{d_w} \quad , \tag{17}$$

where μ_0 is the magnetic permeability of free space (H m^{-1}).

The temperature and volume variation of the capsule have been measured in experiments in which two variables were changed: the environmental temperature of the capsule and the dosage of reactants. The experimental setup is shown in Fig. 5 (b) as well as in the supplementary video.

Experiment A: The first set of experiments was conducted at room temperature of 24 °C in Tank A, and the ratio of the gelatin rings was as in Table I. Tank A, shown in Fig. 5 (b), is a water chamber made of PLA, designed to measure the volume expansion of the capsule. This chamber has a ceiling fixed in place to prevent the capsule from floating after expansion. The ceiling also has holes allowing liquid to rise, so the volume of gas released can be measured via displacement of water. Measurement lines are displayed on a frontal panel of the chamber to track the rise of the water level by a webcam.

The coil is placed underneath the tank at a distance of 4 cm. The temperature outside of the capsule, inside tank A was measured using an LCD thermometer. The water was dyed with blue dye for visual clearance.

Experiment B: The second set of experiments was carried out at the body temperature of $37\,°C$ and the reactants of gelatin rings were 183 mg of $C_6H_8O_7$ and 220 mg of $NaHCO_3$. The tank A apparatus was placed inside Tank B as in Fig. 5 (b). Tank B is a water bath made from acrylic, insulated with a layer of Ecoflex, and the water inside was heated with two electrically insulated $5\,W$ resistors of $22\,\Omega$, connected to a motor controller. A digital thermocouple was used to measure the temperature of the water bath and an Arduino Mega microcontroller connected to the motor controller was used to regulate the temperature of the water bath at around $37\,°C$. An LCD thermometer was used to measure the temperature of the capsule inside tank A and an additional one was placed inside the water bath as control. The same setup for Experiment B was used for testing the time it takes for capsule inflation from frozen at body temperature without any extra heat input, instead of defrosting the capsule back to room temperature before the experiment like in Experiment A and B.

Another experiment was carried out to find out how the pressure and maximum diameter of the capsule changes with volume. A syringe filled with air was connected to the capsule and a pressure sensor (005PGAA5, Honeywell). The sensor collected the pressure data while the maximum diameter of the capsule was measured using a caliper. All experiments above consisted of five trials each. The data gathered was used to calculate the mean and standard deviation.

The capsule navigation in a human intestine phantom was tested using an electromagnetic coil system shown in Fig. 5 (a), based on our previous work [24], [37]–[39] with a total peak magnetic field of $10\,mT$. The intestine phantom was made from Ecoflex-30 with a diameter of $25\,mm$. The speed of navigation was derived from video tracking. To carry out a demonstration of the capsule functionality, the capsule was inserted from one end of the phantom and navigated to the center. Induction heating was applied to the capsule for 30 minutes. After deflation, the capsule was navigated out again.

Lastly, an ex vivo trial was carried out in a sample of pig small intestine. The capsule was placed inside the intestine and tied with a knot at the bottom to prevent the capsule slipping out. The intestine was hung on an arm $4\,cm$ away from the coil. The capsule design was modified to have a hook attached to the bottom to hang weights. When the volume reached maximum inflated size, the knot was removed and weights were incrementally hung until the capsule slipped out to get an estimate of the anchoring force. The capsule was placed back in position and left to continue with the deflation process. Both the phantom and pig intestine trials were carried out at room temperature.

IV. RESULTS AND DISCUSSION

1) Effects of temperature and reactant dose on capsule inflation: Fig. 6 shows the measured results from Experiment A and B while magnetic induction was applied for the first 30
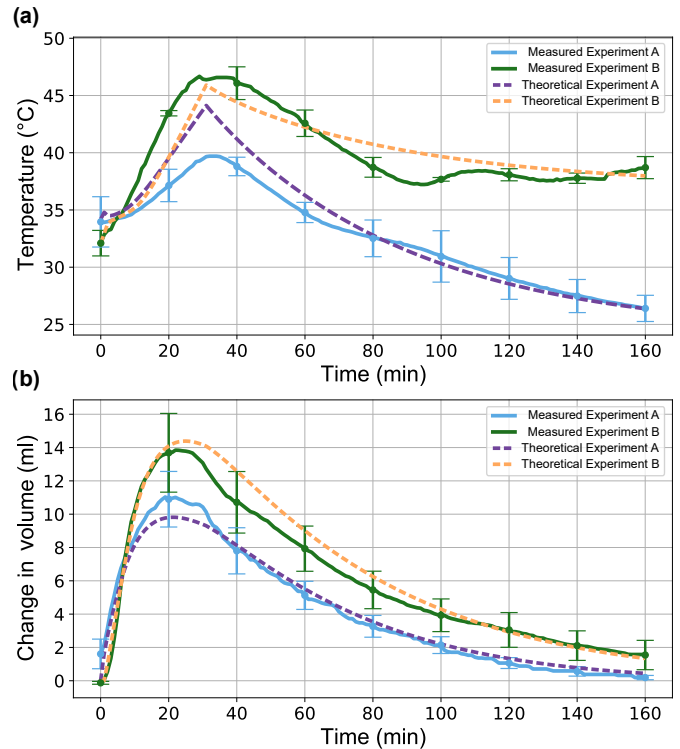

Fig. 6. Two sets of measured trials showing (a) the temperature outside the capsule and (b) inflation and deflation of the capsule. The capsule was heated for the first 30 minutes. The plots show the mean measurements for trials with two sets of conditions. The measured results are compared with the theoretical curve of the simulation when it is run with the same conditions.

minutes. During both trials, temperature next to the capsule and the change in volume of the capsule was measured.

The theoretical plots of temperature and volume from the simulation, generated with the same corresponding experimental conditions, are also presented in Fig. 6 (a) which show similar trends to their measured equivalents. The trials were carried out without a temperature limit and the maximum mean temperature reached during trials from Experiment B was $46.5\,°C$, which is slightly above hyperthermic limits. As the trials from Experiment A show that the capsule can operate below $45\,°C$, the capsule functionality would not be affected if a temperature limit was introduced.

The dilation profile of the capsule, measured across trials with both conditions in Fig. 6 (b) suggests that the actuation pattern is repeatable, with a maximum standard deviation of $1.67\,ml$ for Experiment A and $2.36\,ml$ for Experiment B. In particular, the maximum volume reached for Experiment A and B were $11\,ml$ and $13.8\,ml$ respectively. Comparison of the two means of experiment A and B show that $0.1 > p > 0.05$ for minute 20, and $p < 0.025$ for the rest. Temperature affects both the rate of dissolution and the rate of reabsorption, and the mass of reactants directly affects the amount of CO_2 produced. The theoretical plots of the volume of the capsule follow the measured trends both during inflation and deflation across the varying temperatures through the experiments. The results from this experiment validate the performance of the simulation, with two variables, temperature and mass of reactants, being tested. From the two trials carried out to test the capsule
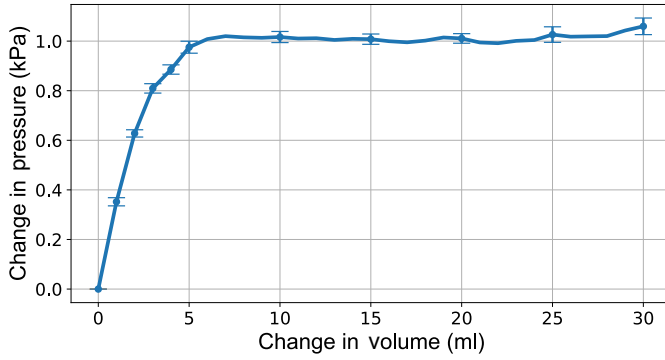
Fig. 7. The pressure and volume relationship of the capsule actuation while unconstrained.
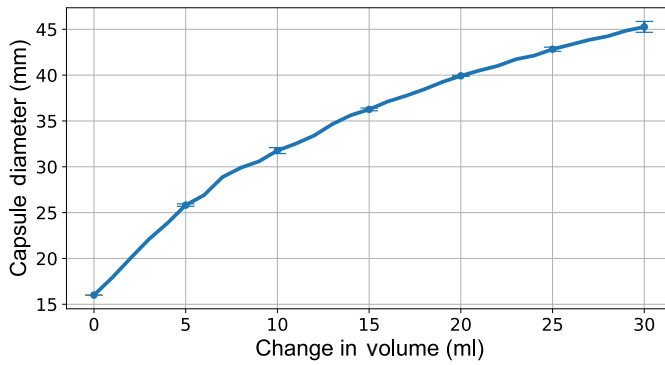

Fig. 8. The diameter and volume relationship of the actuator.

inflation at body temperature from frozen, it resulted that it takes around 5 minutes for the capsule to start inflating, and around 18 minutes for the capsule to reach the diameter of human intestine (30 mm) without extra heat input as opposed to 10 minutes with induction heating. This experiment suggests the time that could be used to navigate the capsule to the site of inflation could be suitable for the first half of the small intestine .e.g., alternative to double balloon endoscopy. Gelatin can be replaced with another material that has a higher melting point than body temperature and is insoluble in water to prevent any actuation before heat input. This comes at the cost of slower response time or higher induction coil power requirements. The same methodology presented in this paper can be used to characterize the inflation behavior with the new material.

2) Relationship between volume, pressure and diameter: Fig. 7 presents the relationship between pressure and volume of the capsule, measured at room temperature. The results were used to derive Eq. 11, which is valid when the capsule is inflating without a constraint. The measurements show that the capsule needs around 1 kPa at 5 ml of volumetric increase to overcome the resistance from the soft membrane, then levels off for volumes within the tested range. Fig. 8 shows how the maximum diameter of the soft membrane changes with volume of gas inside the capsule. Using the results, the diameter of the actuator when the capsule is inflated, d_a, was curve-fitted

for a range of $0 \leqslant V < 30$ ml to derive the formula:

$$d_a = 34.37 e^{9.74 \times 10^{-3} V} - 18.5 e^{-0.112 V} \quad , \qquad (18)$$

where V is the volume of gas inside the actuator (ml). The equation can be used to predict the volume of gas necessary to reach the diameter of a section of the gastrointestinal tract.

3) Navigation and capsule demonstration: The capsule navigation was tested in the human intestine phantom, which is shown in Fig. 9 as well as in the supplementary video. The offset magnet rolls the capsule and propels forwards as the center of gravity and the magnetic potential causes one side of the capsule to raise up and down as the capsule rolls. The crawling speed of the capsule in the phantom was determined to be $2.67\,\mathrm{mm\,s^{-1}}$ from 10 trials. Fig. 9 (a-d) shows the capsule demonstration. The capsule is navigated to the center of the phantom where the induction coil is located. Induction heating is applied to inflate and anchor the capsule. The navigation coils were used to confirm that the capsule has inflated above the diameter of the phantom and anchored by trying to propel the capsule using magnetic fields and show that it does not move at this state. After deflation, the capsule stops anchoring and is moved further down the phantom using the navigation coils.

4) Anchoring on biological tissue: The anchoring capability of the capsule is demonstrated in Fig. 10. The capsule is wirelessly inflated in a section of pig small intestine, whose average diameter is 20 mm [40]. This diameter is smaller compared to human small intestine but should provide closer results to using real human intestine as opposed to using the phantom due to the small friction coefficient intestinal fluids provide and elastic properties of the tissues of human and pig intestine being closer to each other than Ecoflex-30 is. The axial diameter of the capsule increased from 18 mm to 24 mm, which is a smaller increase compared to the previous unconstrained experiments. Since the capsule is in a section of pig intestine, the walls of the intestine apply a reactive force to the capsule. Once the intestine diameter is reached, the constraining force of the intestine will end up increasing the pressure inside the capsule as well rather than mostly increasing its volume. While constrained, the added pressure increases the anchoring force which means volume increase beyond the diameter of the intestine can be interpreted as where the capsule starts anchoring. The capsule was able to inflate enough for dilating the tissue and the anchoring force was measured to be around 0.27 N.

V. CONCLUSIONS

In this paper, an untethered inflatable robotic capsule was presented for tissue dilation. The magnetic induction driven chemical reaction used for the inflation mechanism provides a novel method for controlling inflatable robots. The designed capsule provides volumetric expansion that can be sustained for 44 minutes above 30 mm axial diameter and can operate at temperatures below 45 °C. The study of the mechanism provides different control parameters, which can be used for simulating the actuation behavior and design capsules of varying sizes for different applications. The model developed
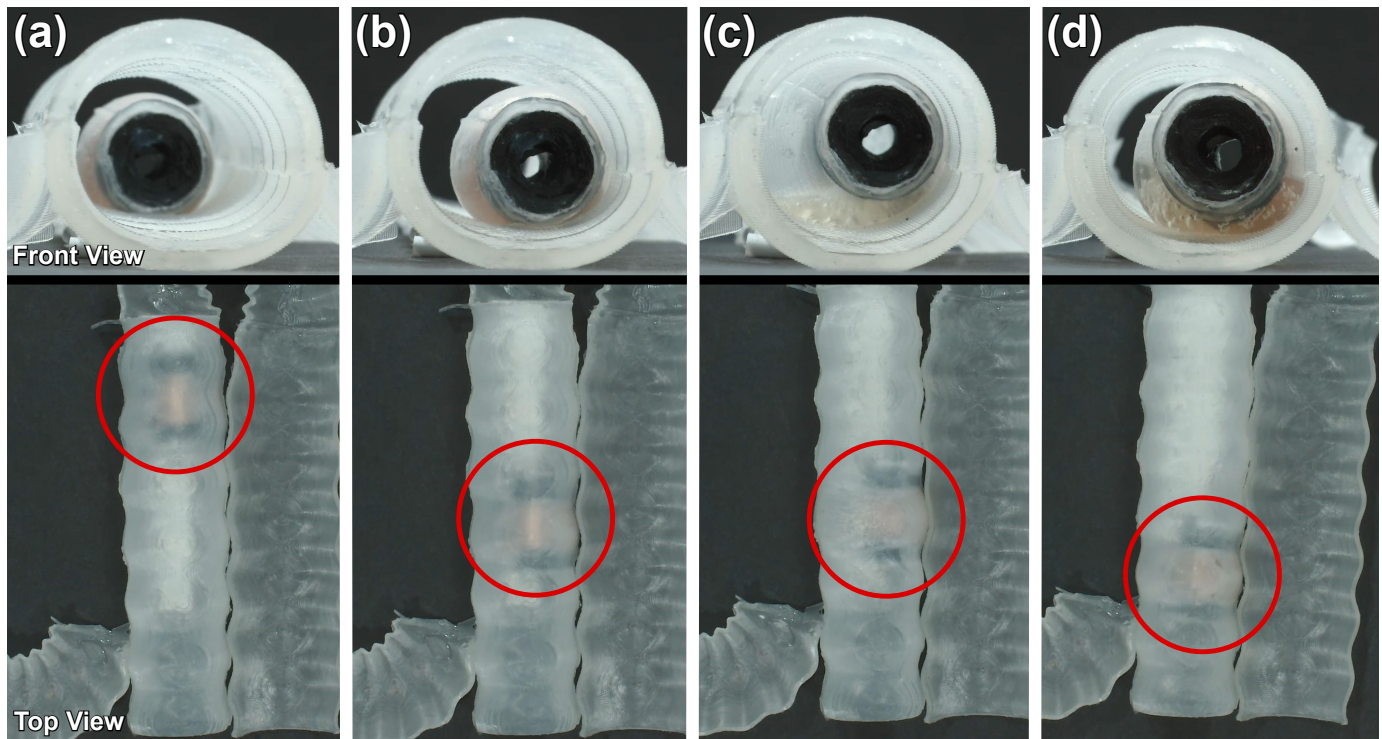
Fig. 9. Demonstration of the capsule navigation and anchoring in an intestine phantom from front view (top images) and top view (bottom images). (a-b) shows the navigation of the capsule down the phantom. The red circles indicate the location of the capsule. (c) The capsule is stationary. Induction heating is applied for 30 minutes to inflate and anchor the capsule. (d) After deflation, the capsule is navigated out.
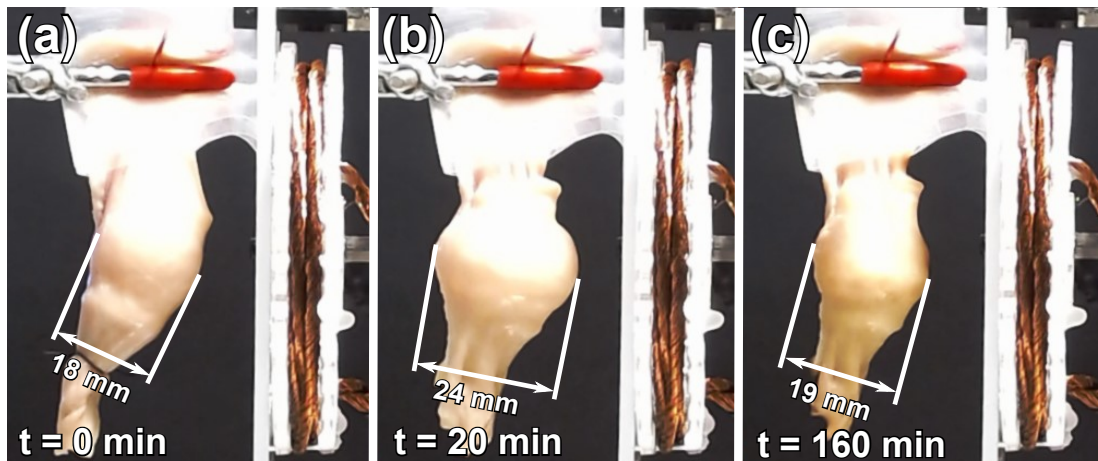

Fig. 10. Shows an ex vivo trial carried out using a section of pig intestine. (a) The capsule was placed inside the intestine with a knot at the bottom to prevent slipping. (b) After 20 minutes of wireless heating, the capsule reaches maximum expansion. Weights were hung on the capsule to test anchoring force. Then the capsule was heated for 10 more minutes and (c) left to deflate.

for the capsule's volume change showed accuracy and can be used to refine the capsule's control. With the parameters chosen for this study, the volumetric expansion of the capsule can be sustained for 44 minutes greater than the axial diameter of an intestine. The chemical actuation of the fabricated capsule as a result of this study achieved an expansion from $16\,\mathrm{mm}$ to $35\,\mathrm{mm}$ with $0.27\,\mathrm{N}$ of anchoring force. Capsule navigation was tested with an electromagnetic coil system and achieved a crawling speed of $2.67\,\mathrm{mm\,s^{-1}}$ in an intestine phantom. The ex vivo trial carried out shows that the force generated by the capsule is sufficient to dilate a section of

pig intestine in order aid surgical operations, and anchor the capsule body. The design and control of the capsule can be deemed safe for in vivo applications given that: the method used for inflation has low risk of harming the patient, the chemicals the inflation is based on is safe for ingestion in the case of a burst, and the capsule has shown a relatively small error of 15.2% for Experiment A and 17.1% for Experiment B. This error is mostly due to fabrication error of gelatin rings as small changes in the reactant amounts can cause a large change in volume behavior of the capsule.

When designing for different applications, the maximum

expanded volume, the rate of volume increase and the time the capsule stays above a certain volume threshold can be adjusted. For example, for stent deployment or mild stricture treatment, the thermal energy input can be increased to decrease the inflation time and increase the pressure output when the capsule is constrained by the stent. The pressure output can be predicted using Eq. 11 and Eq. 18 if the target diameter is known.

The chemical reaction based inflation provides the advantage of untethered devices which open the potential of minimally traumatic surgical treatments. The inflation can be controlled on site by a priori design of the capsule, e.g., amount of reactants, volume of water, and thermal input via induction heating. A limitation of the current actuation approach is that the current chemical reaction is not reversible, thus the inflation cannot be repeated. If multiple inflation-deflation cycles are needed, then a reversible chemical reaction, or alternative methods should be sought [20], [41]. If the distance of the induction coil from the capsule needs to be increased depending on clinical needs, the current provided to the induction coil can be increased such that the amplitude of the magnetic field received by the capsule stays constant. To improve biocompatibility, the rigid body and rigid cap can be replaced with any biocompatible rigid material and cyanoacrylate can be replaced with a medical grade one. We will also seek to miniaturize the design by reducing the diameter by 31.3% to fit a standard capsule size "000". Future work will look at adjustment of the design to fit clinical requirements and its evaluation in more complex biological models.

Acknowledgment

References

[1] M. F. Hale, R. Sidhu, and M. E. McAlindon, "Capsule endoscopy: current practice and future directions," *World journal of gastroenterology*, vol. 20, no. 24, pp. 7752–7759, Jun 2014.

[2] D. Ye, J. Xue, S. Yuan, F. Zhang, S. Song, J. Wang, and M. Q.-H. Meng, "Design and control of a magnetically-actuated capsule robot with biopsy function," *IEEE Transactions on Biomedical Engineering*, vol. 69, no. 9, pp. 2905–2915, 2022.

[3] N. K. Mandsberg, J. F. Christfort, K. Kamguyan, A. Boisen, and S. K. Srivastava, "Orally ingestible medical devices for gut engineering," *Advanced Drug Delivery Reviews*, vol. 165-166, pp. 142–154, 2020.

[4] F. Munoz, G. Alici, and W. Li, "A review of drug delivery systems for capsule endoscopy," *Advanced Drug Delivery Reviews*, vol. 71, pp. 77–85, 2014.

[5] P. R. Slawinski, K. L. Obstein, and P. Valdastri, "Emerging issues and future developments in capsule endoscopy," *Techniques in Gastrointestinal Endoscopy*, vol. 17, no. 1, pp. 40–46, 2015.

[6] Y. L. Kong, X. Zou, C. A. McCandler, A. R. Kirtane, S. Ning, J. Zhou, A. Abid, M. Jafari, J. Rogner, D. Minahan, J. E. Collins, S. McDonnell, C. Cleveland, T. Bensel, S. Tamang, G. Arrick, A. Gimbel, T. Hua, U. Ghosh, V. Soares, N. Wang, A. Wahane, A. Hayward, S. Zhang, B. R. Smith, R. Langer, and G. Traverso, "3d-printed gastric resident electronics," *Advanced Materials Technologies*, vol. 4, no. 3, p. 1800490, 2019.

[7] S. M. Mirvakili and R. Langer, "Wireless on-demand drug delivery," *Nature Electronics*, vol. 4, no. 7, pp. 464–477, 2021.

[8] A. Abramson, E. Caffarel-Salvador, V. Soares, D. Minahan, R. Y. Tian, X. Lu, D. Dellal, Y. Gao, S. Kim, J. Wainer, J. Collins, S. Tamang, A. Hayward, T. Yoshitake, H.-C. Lee, J. Fujimoto, J. Fels, M. R. Frederiksen, N. Rahbek, Ulrikand Roxhed, R. Langer, and G. Traverso, "A luminal unfolding microneedle injector for oral delivery of macromolecules," *Nature Medicine*, vol. 25, no. 10, pp. 1512–1518, Oct 2019.

[9] K. Wang, J. Ma, F. Wang, Z. Wang, G. Yan, and Y. Zhou, "Full-driving soft robotic colonoscope in compliant colon tissue," *J. Med. Eng. Technol.*, vol. 41, no. 8, pp. 662–669, Nov. 2017.

[10] R. M. Bonnor and K. A. Ludwig, "Laparoscopic colectomy for colon cancer: comparable to conventional oncologic surgery?" *Clin. Colon Rectal Surg.*, vol. 18, no. 3, pp. 174–181, aug 2005.

[11] C. J. Fyock and P. V. Draganov, "Colonoscopic polypectomy and associated techniques," *World journal of gastroenterology*, vol. 16, no. 29, p. 3630–3637, 2010.

[12] O. Onaizah and E. Diller, "Tetherless mobile micro-surgical scissors using magnetic actuation," in *2019 International Conference on Robotics and Automation (ICRA)*, 2019, pp. 894–899.

[13] A. Lim, A. Schonewille, C. Forbrigger, T. Looi, J. Drake, and E. Diller, "Design and comparison of magnetically-actuated dexterous forceps instruments for neuroendoscopy," *IEEE Transactions on Biomedical Engineering*, vol. 68, no. 3, pp. 846–856, 2021.

[14] H. Suzuki and R. J. Wood, "Origami-inspired miniature manipulator for teleoperated microsurgery," *Nature Machine Intelligence*, vol. 2, no. 8, pp. 437–446, 2020.

[15] D. Jain, A. Goyal, and S. Zavala, "Predicting colonoscopy time: A quality improvement initiative," *Clinical Endoscopy*, vol. 49, no. 6, pp. 555–559, 2016.

[16] H. Kang and M. H. Thoufeeq, "Size of colorectal polyps determines time taken to remove them endoscopically," *Endoscopy International Open*, vol. 6, no. 5, pp. E610–E615, 2018.

[17] S. Song, S. Yuan, F. Zhang, J. Su, D. Ye, J. Wang, and M. Q.-H. Meng, "Integrated design and decoupled control of anchoring and drug release for wireless capsule robots," *IEEE/ASME Transactions on Mechatronics*, vol. 27, no. 5, pp. 2897–2907, 2022.

[18] L. Yan, T. Wang, D. Liu, J. Peng, Z. Jiao, and C.-Y. Chen, "Capsule robot for obesity treatment with wireless powering and communication," *IEEE Transactions on Industrial Electronics*, vol. 62, no. 2, pp. 1125–1133, 2015.

[19] S. M. Mirvakili, D. Sim, I. W. Hunter, and R. Langer, "Actuation of untethered pneumatic artificial muscles and soft robots using magnetically induced liquid-to-gas phase transitions," *Science Robotics*, vol. 5, no. 41, 2020.

[20] Y. Tang, M. Li, T. Wang, X. Dong, W. Hu, and M. Sitti, "Wireless miniature magnetic phase-change soft actuators," *Advanced Materials*, 2022.

[21] A. Bhardwaj, K. Parekh, and N. Jain, "In vitro hyperthermic effect of magnetic fluid on cervical and breast cancer cells," *Scientific Reports*, vol. 10, no. 1, p. 15249, Sep 2020.

[22] A. E. Deatsch and B. A. Evans, "Heating efficiency in magnetic nanoparticle hyperthermia," *Journal of Magnetism and Magnetic Materials*, vol. 354, pp. 163–172, 2014.

[23] K. Esendag, M. E. McAlindon, D. Rus, S. Miyashita, and D. D. Damian, "Development of an untethered inflatable capsule robot for stricture dilation - a preliminary study," in *Hamlyn Symposium on Medical Robotics 2023*, 15, June 2023, pp. 101–102.

[24] S. Miyashita, S. Guitron, K. Yoshida, S. Li, D. D. Damian, and D. Rus, "Ingestible, controllable, and degradable origami robot for patching stomach wounds," in *2016 IEEE International Conference on Robotics and Automation (ICRA)*, 2016, pp. 909–916.

[25] U.S. Food and Drug Administration, "Code of federal regulations, title 21, volume 3, section 184.1033," 1994.

[26] ——, "Code of federal regulations, title 21, volume 3, section 184.1736," 1983.

[27] S. R. Khan, S. K. Pavuluri, G. Cummins, and M. P. Y. Desmulliez, "Wireless power transfer techniques for implantable medical devices: A review," *Sensors*, vol. 20, no. 12, 2020.

[28] Z. Jia, G. Yan, Y. Shi, and B. Zhu, "A wireless power transmission system for an active capsule endoscope for colon inspection," *J. Med. Eng. Technol.*, vol. 36, no. 5, pp. 235–241, Jul. 2012.

[29] G. Kiran, I. Yilmaz, S. Aydin, F. Sanlikan, and E. Ozkaya, "The shortest distance between the skin and the peritoneal cavity is obtained with fascial elevation: a preliminary prospective laparoscopic entry study," *Facts Views Vis Obgyn*, vol. 14, no. 2, pp. 171–175, Jun. 2022.

[30] F. Fiorillo, *Soft Magnetic Materials in Characterization and Measurement of Magnetic Materials*. Elsevier, 2004.

[31] H. B. Bohidar, "Hydrodynamic properties of gelatin in dilute solutions," *Int. J. Biol. Macromol.*, vol. 23, no. 1, pp. 1–6, Jul. 1998.

[32] J. Kestin, M. Sokolov, and W. A. Wakeham, "Viscosity of liquid water in the range -8 °c to 150 °c," *Journal of Physical and Chemical Reference Data*, vol. 7, no. 3, pp. 941–948, 1978.

[33] B. T. Smith, *Solubility and Dissolution in Remington Education: Physical Pharmacy*. London: Pharmaceutical Press, 2016.

[34] W. J. Bae, J. B. Choi, K. S. Kim, S. J. Kim, H. J. Cho, U. S. Ha, S. H. Hong, J. Y. Lee, and S. W. Kim, "Ab168. evaluation of the biocompatibility of packing materials for a catheter," *Translational Andrology and Urology*, vol. 4, no. Suppl 1, 2015.

[35] Y. Yang, J. Wang, L. Wang, Q. Wu, L. Ling, Y. Yang, S. Ning, Y. Xie, Q. Cao, L. Li, J. Liu, Q. Ling, and J. Zang, "Magnetic soft robotic bladder for assisted urination," *Science Advances*, vol. 8, no. 34, 2022.

[36] H. Yuk, C. E. Varela, C. S. Nabzdyk, X. Mao, R. F. Padera, E. T. Roche, and X. Zhao, "Dry double-sided tape for adhesion of wet tissues and devices," *Nature*, vol. 575, no. 7781, pp. 169–174, Nov 2019.

[37] J. Liu, H. Sugiyama, T. Nakayama, and S. Miyashita, "Magnetic sensor based topographic localization for automatic dislocation of ingested button battery," in *2020 IEEE International Conference on Robotics and Automation (ICRA)*, 2020, pp. 5488–5494.

[38] J. Liu, X. Chen, Q. Lahondes, K. Esendag, D. Damian, and S. Miyashita, "Origami robot self-folding by magnetic induction," in *2022 IEEE/RSJ International Conference on Intelligent Robots and Systems (IROS)*, 2022, pp. 2519–2525.

[39] J. Han, D. Rus, and S. Miyashita, "Roblets: Robotic tablets that self-assemble and self-fold into a robot," in *2023 IEEE/RSJ International Conference on Intelligent Robots and Systems (IROS)*, 2023, pp. 4709–4714.

[40] H. Tang and M. Mayersohn, "Porcine prediction of pharmacokinetic parameters in people: A pig in a poke?" *Drug Metabolism and Disposition*, vol. 46, no. 11, pp. 1712–1724, 2018.

[41] M. Adami and A. Seibel, "On-board pneumatic pressure generation methods for soft robotics applications," *Actuators*, vol. 8, no. 1, 2019.